Peer-reviewed version available at Sensors 2019, 19, 3797; doi:10.3390/s19173797

Article

BCI Gaze Sensing Method Using Low Jitter Code Modulated VEP

Ibrahim Kaya[1]*, Jorge Bohorquez[1] and Ozcan Ozdamar [1]

[1] Biomedical Engineering Department, University of Miami, Coral Gables, FL 33146, USA

* Correspondence: ixk133@miami.edu;

Abstract: Visual Evoked Potentials (VEPs) are used in clinical applications in ophthalmology, neurology and extensively in brain computer interface (BCI) research. BCI literature covers steady state VEP (SSVEP) and code modulated VEP (c-VEP) BCIs along with sophisticated methods to improve information transfer rates (ITR). There is a gap of knowledge regarding the VEP adaptation dynamics, physiological generation mechanisms and relation with BCI performance. A simple dual display VEP switch was developed to test signatures elicited by non-isochronic, non-singular, low jitter stimuli at the rates of 10, 32, 50 and 70 reversals per second (rps). Non-isochronic, low-jitter stimulation elicits Quasi-Steady-State VEPs (QSS-VEPs) that are utilized for simultaneous generation of transient VEP and QSS-VEP. QSS-VEP is a special case of c-VEPs and it is assumed that it shares the similar generators of the SSVEPs. Eight subjects were recorded and the performance of the overall system was analyzed by means of Receiver Operating Characteristic (ROC) curves, accuracy plots and ITRs. In summary QSS-VEPs performed better than transient VEPs. It was found that in general 32rps stimulation had the highest ROC area, accuracy and ITRs in general. To investigate the reasons behind this, adaptation dynamics of transient VEPs and QSS-VEPs at all four rates were analyzed and speculated. Moreover, QSS-VEPs were found to lead to higher accuracy by the template matching compared to SSVEPs at 10rps and 32rps.

Keywords: Gaze Sensing; SSVEP; BCI; c-VEP; transient VEP; QSS-VEP; Deconvolution;

1. Introduction

Recently Brain Computer Interface (BCI) research has shown a remarkable progress as witnessed by an increasing number of publications. BCI provides a direct communication and control channel between the human brain and output devices in order to achieve a desired output function by using the control signals derived from the human brain [1]. Most of the BCI research is focused on increasing the Information Transfer Rate (ITR). Depending on the signal acquisition methods, EEG based BCIs are getting more and more attention due to non-invasiveness and practical EEG headsets available in the market. In EEG based BCI applications there are four main signal classes, namely Slow Cortical Potentials (SCP), Sensorimotor Rhythms (SMR), P300 Evoked Potentials and Visual Evoked Potentials (VEP) [2]. VEP based BCIs paradigms are common due to several advantages. These are mainly high ITR, simple setup, and little user training [3].

VEPs are named after stimulation types such as flash VEP, pattern reversal VEP, pattern-onset-offset VEP [4]. In clinical testing pattern-reversal VEP is the most preferred one due to having least variability in the waveform , latencies and motion [5]. VEP stimulus can be modulated by space, time, luminance, contrast, color, pattern, depth [5]. VEPs can be grouped into two depending on the stimulation rate. At low stimulation rates (< 3-4 reversals per second (rps)) electrical activity on the occipital scalp elicits abrupt changes by the contrast reversing stimulus and then settles until the presentation of the next stimulus. This type of VEP is called 'transient VEP' (TR-VEPs) [6-7]. However

if the stimulus presented at a higher rate and the response contains frequency components constant in amplitude and phase, then it is called 'Steady State Evoked Potentials or SSEP [8-10].

Depending on VEP modulation, three main VEP BCI types exist: time modulated VEP (t-VEP) BCI, frequency modulated VEP (f-VEP) BCI and pseudorandom code modulated VEP (c-VEP) BCI [11]. Both f-VEP and c-VEP BCIs produce high ITRs. Steady state VEP (SSVEP) (f-VEP) based BCIs have advantages of easy system configuration, excellent SNR, immunity to interferences, minimal user training, easy quantification and high ITR [1,11-16]. However, possible target frequencies are limited due to computer display refresh rates limitations and the SSVEP have low amplitudes at high stimulation rates [1, 12, 16].

Pseudo random binary sequences (PRBS) based c-VEP BCI paradigm offers promising results in terms of the ITR, accuracy, and use of many targets in applications [2,11,17]. Even though PRBS are mostly used in system identification, they are also used in physiological applications such as deconvolution and BCI. One particular PRBS, the maximum length sequences or m-sequences were used by Sutter in a BCI application [18]. Although m-sequences have a-priori remarkable noise attenuation due to its sharp autocorrelation properties, they do not provide the expected SNR improvement in physiological recordings due to adaptation [19]. Working on BCI applications, Bin Bin et al. [17], found that when a stimuli with sharp autocorrelation is used, the physiological system generates responses with lower autocorrelation sharpness, significantly reducing the a-priori effectivity of that BCI system. Therefore, the knowledge of the adaptation characteristics of the visual system should be integrated in the design of the whole BCI system to achieve optimal performance.

Low-jitter PRBS have been successfully used to unveil the unitary responses of the visual system through Pattern Electroretinograms and VEPs [20-21]. Low jitter stimuli elicit c-VEPs with narrow spectrum, similar to the SSVEP and named as Quasi SSVEP (QSS-VEP); they have unique features such as capability for deconvolution of transient VEPs (TR-VEPs), immunity to adaptation, and shared brain generators of the SSVEP.

The use of a physiologically adapted low jitter PRBS stimuli in a BCI gaze sensor may capture advantages of both f-VEPs and c-VEPs paradigms reducing their shortcomings. For this reason, in this study, we developed a dual display BCI gaze sensor based on specially designed low-jitter PRBS codes eliciting QSS-VEP and adopted the template matching as the detection method.

2. Materials and Methods

Right and left gaze sensing systems were developed using two independent regions (right and left) on a fast Visual Display Unit (VDU). Four stimulation rates (10, 32, 50 and 70rps) were explored on a normal subject population. For each rate, detection was evaluated using QSS-VEP and TR-VEPs. For the rates of 10 and 32 rps the SSVEPs were also evaluated. 50 and 70rps SSVEPs were excluded due to low amplitudes [22]. Using raw EEG recordings, the system performance, in all conditions, was quantified off-line by using ROC curves, areas under the curves (AUC), accuracies and ITRs.

2.1. Subjects

Total 8 subjects (5M, 3F) with no history of neurological impairment participated in this study. The subject ages ranged from 18 to 31. All the subjects had either normal or corrected-to normal vision and were right eye dominant. They signed informed consent forms approved by University of Miami Institutional Review Board (IRB) prior to the participation.

2.2. Stimuli Design and Stimulator Display

The display consisted of two fast switching on demand LED based regions for left (Left Field, LF) and right targets (Right Field, RF) (Figure 1). Subjects were placed 1 meter away from the stimulator display to ensure the target displays lie in foveal field of view. Stimulator provided two target stimuli, each covering a visual field of 5.7° x 5.7°. The luminance of the display was 580 Cd/m^2. The stimulus pattern of the targets consisted of 12 horizontal black and white bars with spatial frequency of 1.03 cycles/degree. Right and left regions were driven by two stimuli of slightly different

Peer-reviewed version available at Sensors 2019, 19, 3797; doi:10.3390/s19173797

length and jitter but similar rate (Table 1). Low jittered, low noise amplification sequences similar to were used [20-21, 23]. These sequences have low jitter and thus resemble the steady state isochronic stimulation sequences. Moreover they are non-singular in frequency domain and allow deconvolution to extract transient VEPs (See [8] for deconvolution). A cue light blue for Left, red for Right, green for Center was lit for indication of gaze direction to the subjects.

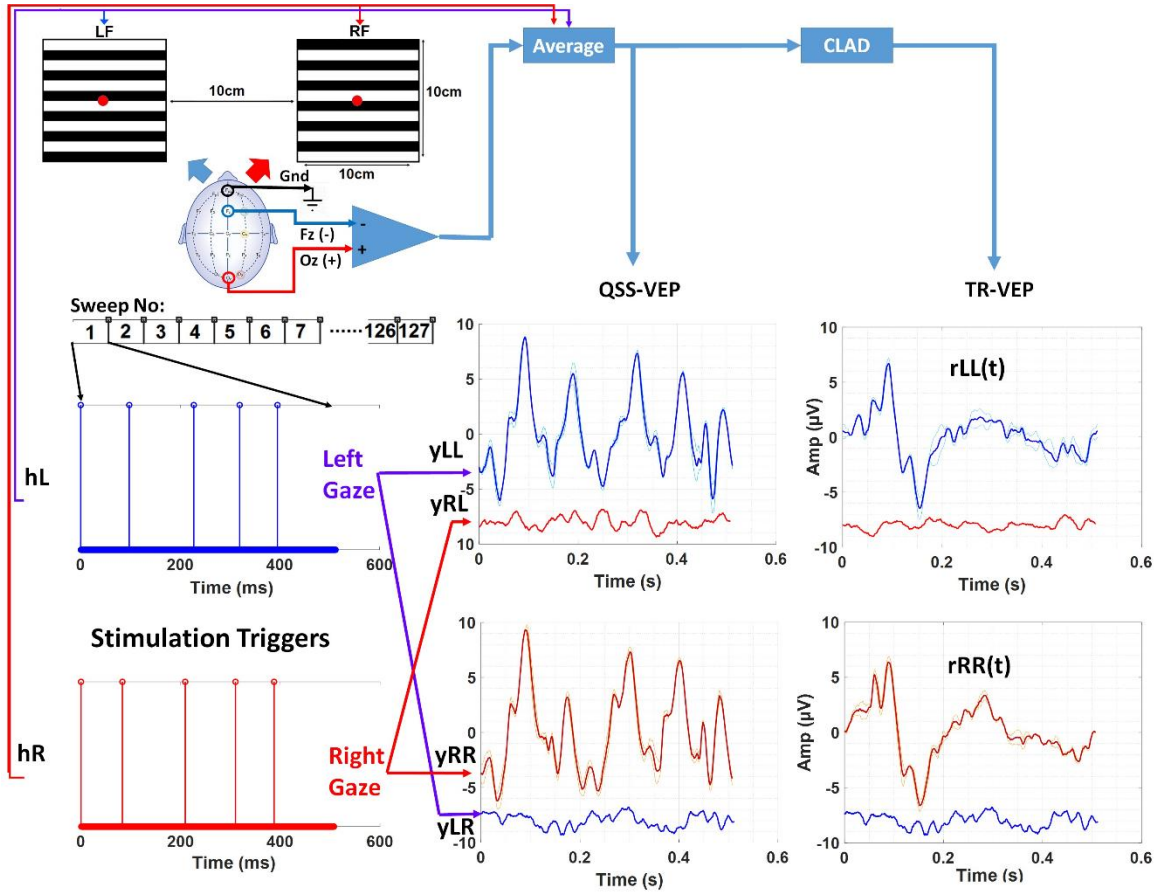

Figure 1. Overall system setup and experimental procedure is shown for 10rps stimulation. Stimulator is shown at the top left, driving sequences for left field (LF) and right field (RF) are shown at the bottom left, the QSS and transient responses from subject 5 are shown in the bottom right figures. Interference signals after averaging 127/128 sweeps in one file for left/right, yRL and yLR, are also displayed to highlight the orthogonality of the sequences.

2.3. Experimental Setup and EEG Recording

Single EEG channel was recorded using Oz as positive, Fz as negative and forehead as ground. Three passive Ag/AgCl electrodes were used in the experiments. Electrode impedances were checked and kept below 7kΩ. EEG was recorded with an Intelligent Hearing System (IHS, USA) data acquisition module (16 bits) at sampling rate of 2 kHz. Analog signal was bandpass filtered with 1-300Hz (6db/octave) filters. Raw EEG data along with stimulation triggers and synchronization cues were stored for off-line analysis.

Peer-reviewed version available at Sensors 2019, 19, 3797; doi:10.3390/s19173797

Table 1. Stimulation Properties for QSS and SS stimulation paradigms.

Signal	Nominal Rate (rps)	Mean Rate (rps)	Field	Sweep Duration (ms)	Sweep Count	File Acquisition Time(s)	Template Acquisition Time(s)
QSS	10	9.76	LF	512	127	64.0	128.0
		9.84	RF	508	128	64.0	128.0
QSS	32	31.25	LF	512	31	15.9	47.6
		30.25	RF	496	32	15.9	47.6
QSS	50	49.6	LF	504	62	31.2	62.5
		52.4	RF	496	63	31.2	62.5
QSS	70	70.5	LF	496	32	15.9	47.6
		70.3	RF	512	31	15.9	47.6
SS	10	10	LF	500	39	19.5	39.0
		10.5	RF	487.5	40	19.5	39.0
SS	32	31	LF	512	31	15.9	47.6
		32	RF	496	32	15.9	47.6

The rate study consisted of two sessions, first one was training (template generation) and second session was system performance evaluation. During the rate experiment, each rate single file acquisition durations (Table 1) were different. Hence for 10, 32, 50 and 70rps, 2 files, 3 files, 2 files and 3 files were recorded respectively to generate templates in training session for left and right gazes. Same number of files were recorded for the second session for testing purpose. The acquisition order was 10rps, 32rps, 50rps and 70rps consecutively. Template acquisition was done by averaging EEG sweeps, for number of sweeps refer Table 1. During the recordings the operator monitored the experiment to ensure signal quality , no powerline interference, subject's cooperation, subject's gaze. In the event of poor cooperation by subject, sleepiness or excessive eye blinks , the recording was halted and either repeated or postponed for another time. Between recordings, subjects had 30s rest intervals.

2.4. EEG Offline Processing

The EEG epochs/sweeps in the same condition files were averaged in MATLAB 2018b (MathWorks, USA) environment except for the sweeps with peak to peak amplitudes > 80μV. Those large peak to peak sweeps were discarded. In this averaging, +/- averaging, noise and Signal to Noise Ratio (SNR) computations were also carried out.

For one cycle/file of stimulation when the subject gazed at one stimulation region, the response to the other stimulation region is almost zero due to orthogonality which can be seen from yRL(red) and yLR(blue) plots in Figure 1 .

Left and right display regions were driven by hL and hR stimulation sequences respectively as shown in Figure 1. The 10rps QSS-VEPs for left and right regions were obtained by averaging the EEG data with window lengths of 1024 and 1016 points or 512ms and 508ms windows. For the other reversal rates the window sizes or sweep durations are given in Table 1. The QSS-VEP responses are hypothesized to result from convolution of the stimulation sequences hL or hR and ideal transient response at that particular adaptation rate. This can be seen from equations 1 and 2.

$$y_{LL}(t) = h_L(t) * r(t) \Rightarrow Y_{LL}(f) = H_L(f) * R(f) \quad (1)$$

$$y_{RR}(t) = h_R(t) * r(t) \Rightarrow Y_{RR}(f) = H_R(f) * R(f) \quad (2)$$

The deconvolution can be applied since stimulation sequences hL and hR are nonsingular. Then the transient responses for right field stimulation and right gaze is rRR(t) and left field stimulation and left gaze is rLL(t) which were obtained by deconvolution and inverse fast fourier transform (ifft) are almost identical due to very similar stimulation sequences and adaptation as seen from equations 3 and 4.

$$R_{RR}(f) = \frac{Y_{RR}(f)}{H_R(f)} \Rightarrow r_{RR}(t) = ifft\left(\frac{Y_{RR}(f)}{H_R(f)}\right) \quad (3)$$

$$R_{LL}(f) = \frac{Y_{LL}(f)}{H_L(f)} \Rightarrow r_{LL}(t) = ifft\left(\frac{Y_{LL}(f)}{H_L(f)}\right) \quad (4)$$

By averaging the multiple EEG data segments of left or right sequence lengths, it was possible to extract QSS-VEP responses to right and left targets (see Figure 1) for different data sizes. Since stimulation sequences were nonsingular, deconvolution method in frequency domain was applied to obtain TR-VEP responses. QSS-VEP and TR-VEP templates were computed by averaging the two EEG files for 10rps and 50rps, similarly three EEG files for 32rps and 70rps for each gaze direction.

2.5. Gaze Detection and ROC Estimation

Gaze detection process involved cross-correlation between the reference templates and the signal. We utilized Pearson's product-moment correlation coefficient between subject's template VEP and subject's actual test data in our method. The correlation coefficient was compared to a threshold for decision. If the correlation coefficient was higher than threshold, the signal matched the template's gaze direction. For this purpose templates for each gaze and rate condition were extracted following the training sessions. Proper calculation and selection of threshold values from cross correlation coefficients were critical in the gaze detection. ROC is a curve representing the performance of the classifier. By change of operation threshold value, ROC determines the probability of error and accuracy (true positive ratio) in system. After the files recorded and templates ready to be used in comparison, ROC curves were calculated in order to evaluate the performance of the classifier. To compute ROC curves two classes of files (left and right gaze files) were fed into an algorithm where left or right templates were used as references. Since file gaze conditions were known, true positives, false positives, true negatives, false negatives were available while threshold was varied from -1 to 1 by steps of 0.05 for correlation coefficient. ROC curves were computed for 0.5s, 1s, 1.5s, 2s, 2.5s, 3s, 3.5s, 4s of data length.

3. Results

Overall system performance was evaluated by offline analysis. This covered ROC curves and areas, accuracies, ITR computations, plots and comparisons. Generally t-test paired two sample for means was used to examine the effects of various conditions on the performance, particularly on accuracy and ITR. The effect of gazing left or right stimulus was tested by computing accuracies. It has been found that statistically there is no significant difference in the mean accuracies by left or right gaze using single sweep (0.5s) QSS-VEP signature at all rates. Therefore for the same conditions left and right gazed performances were averaged in order to generate a single parameter to represent the performance at that particular condition. This reduced the number of comparisons hence complexity in the analysis.

There were many signatures to test the system performance with. For 10rps stimulation these were mainly the combinations of right and left , QSS-VEP and TR-VEP responses. It followed the same signatures for 32rps, 50rps and 70rps stimulation. By averaging left and right QSS-VEP performances in terms of accuracy or ROC area, an average accuracy or ROC area was computed for each rates of QSS (10, 32, 50, 70rps) and steady state (SS) conditions (10 and 32rps).

3.1. VEP Morphology by Rate Adaptation

The recording electrode sites might reveal different signals depending on the adaptation characteristics of dominant neural populations over the particular sites [24]. Four rates of 10rps, 32rps, 50rps and 70rps QSS-VEPs are shown in Figure 2-A, it can be seen that 70rps QSS-VEP has smaller peaks compared to others. In Figure 2-B, transient TR-VEP waveforms are shown. While 10rps TR-VEP has characteristic early peaks and negativities, 32rps, 50rps and 70rps have totally different waveforms. There a positive peak replaces the negativity around 120-150ms. When we compare the TR-VEP amplitudes, 32rps has the largest amplitude 12µV, 50rps has 10.9µV, 10rps has 10.5µV, and 70rps has the minimum 5.2µV amplitude.

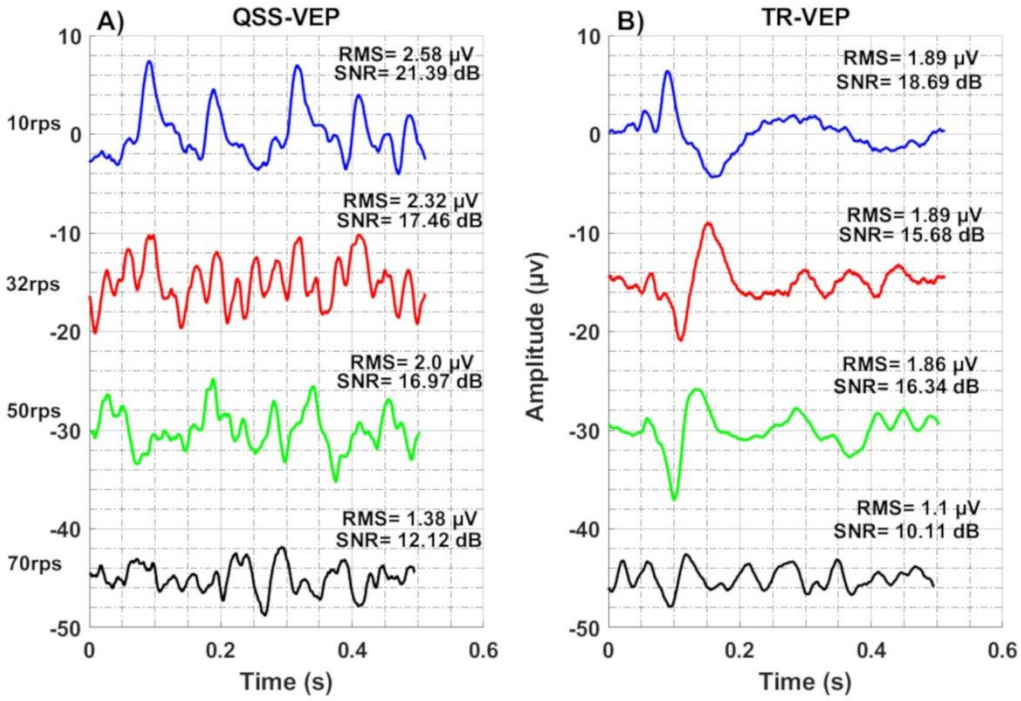

Figure 2. Population average left field QSS-VEP and TR-VEP plots are shown. A) 10rps, 32rps ,50rps and 70rps QSS-VEPs are at the left. B) TR-VEPs are at the right. Note the morphology change in the TR-VEPs by rate from 10rps to 32rps.

3.2. Offline Analysis and Performance

Template matching was adopted as the method for target recognition. Threshold values for right and left target detection were pulled from ROC curves as the threshold index value corresponding to max ROC AUC. Once thresholds were set and template signals were uploaded, files with known status were tested with system and the results were plotted.

There are many metrics to evaluate the performance of a BCI system. Thompson et al. 2013 compared these metrics of accuracy or error rate, Cohen's Kappa coefficient, confusion matrix, mutual information and ITR in terms of throughput, categorical output, unbiased/biased, practicality [25]. They suggested ITR as optimum metric for level-1 BCI system. Our system was tested offline with QSS-VEP and TR-VEP signatures and for all stimulation rates. ITR and accuracies were used in this evaluation. ITR can be calculated by the following equation 5:

$$ITR = \left[log_2(N) + P\ log_2(P) + (1-P)\ log_2\left(\frac{1-P}{N-1}\right)\right]\frac{60}{T} \quad (5)$$

P is the probability of correct selection, N is the number of choices and T (seconds/selection) time required to select a choice/target [25]. Its unit is given in bits per minute (bpm). ITR simply follows the accuracy of the classification, the higher the accuracy the bigger is the ITR. There is a limit of ITR

by selection time and maximum accuracy of 1. For a two target system, at maximum accuracy ITR is 60 / (selection time).

In the experiments subject 6 achieved a remarkable accuracy of 0.96 and corresponding ITR of 93bpm at 32rps 0.5s data and QSS-VEP right gazing BCI switch condition. QSS-VEP and TR-VEP ROC curves for 50rps and left gaze conditions were compared. For data durations 0.5s, 1.5s and 2.5s, 50rps ROC areas were found as 0.86, 0.92 and 0.95 respectively for left QSS signal. Similarly for left TR-VEP, 0.5s, 1.5s and 2.5s data durations, accuracies were 0.73, 0.80 and 0.83 respectively. It should be noted that the ROC area increases by increase of data size. Inclusion of extra sweeps in the average increases the SNR and better ROC area and accuracy are achieved.

When ROC curves for QSS-VEP and TR-VEPs were compared, QSS-VEPs were found to perform better than TR-VEPs for 10rps stimulation ($p<0.05$) (See Figure 3) . Classifier performances for TR-VEPs using 0.5s - 1 sweep data were compared in Figure 3-b. The low performance with 10rps can be attributed to the alpha band activity interference which was reported in [22] and [26]. It can be seen from the Figure 3 that among S3 ROC curves for different rates, 32rps has the largest ROC area for both left QSS-VEP and left TR-VEP. 10rps and 50rps have similar ROC areas for QSS-VEP, 70rps has the minimum ROC area for both QSS-VEP and TR-VEP which summarizes the system performance at these rates. The QSS-VEP paradigm boosts the ROC area performances obtained by TR-VEPs by 14% for 10rps for S3.

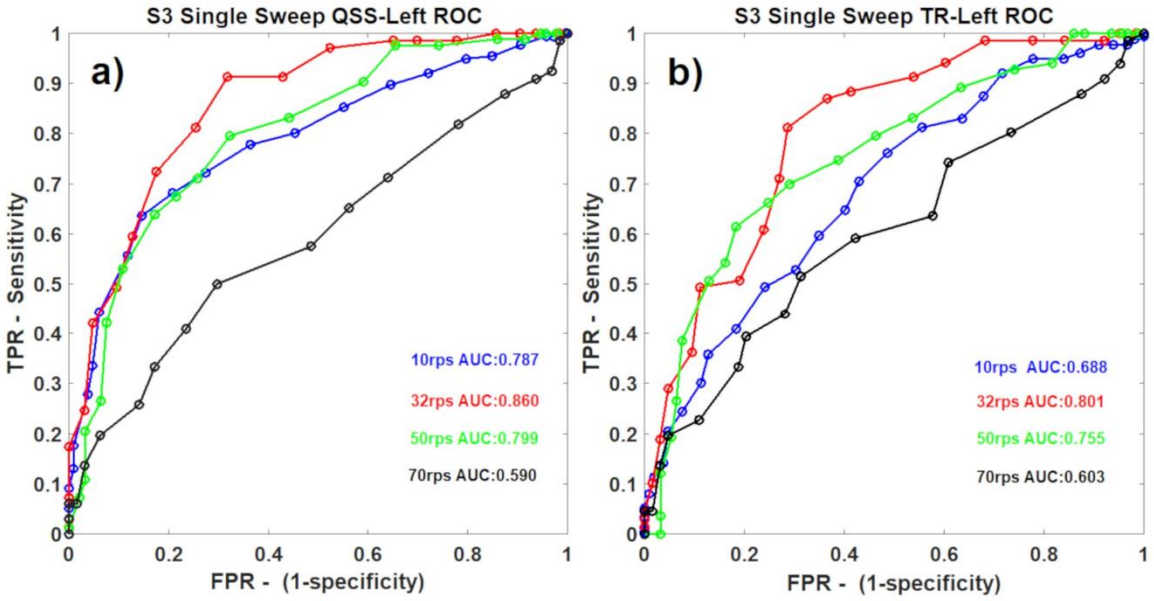

Figure 3. S3 single sweep 0.5second condition. **a)** Left QSS-VEP ROC curves and areas for all the rates are shown at the left. **b)** Left TR-VEP ROC curves and areas for all the four rates are shown at the right.

When we compare the accuracy table with QSS-VEP rms table given in the supplementary table S1, there is a relation that increasing QSS-VEP rms increases the accuracy. However the relation between SNR and accuracy is more prominent. With QSS-VEP rms and accuracies averaged for each subject, we found correlation coefficients of 0.72 for 1s and 0.70 between rms values and accuracies for 0.5s data. On the other hand the correlation coefficient between the subject average SNR and accuracies are 0.94 and 0.92 for 1s and 0.5s data respectively.

As mentioned before in this paper, the left and right QSS-VEP performances are combined to create a single parameter for that condition which reveals the rate dependent characteristics easily in one figure. See Figure 4 for the rate effect on QSS-VEP and TR-VEP signals. It was found that for QSS-VEP 32rps had the biggest accuracy and ITR among all rates for 0.5s data. QSS-VEP ITRs are bigger than TR-VEP ITRs. On the other hand TR-VEP ITR performances can be seen from the bottom

Preprints (www.preprints.org) | NOT PEER-REVIEWED | Posted: 9 July 2019 doi:10.20944/preprints201907.0128.v1

Peer-reviewed version available at Sensors 2019, 19, 3797; doi:10.3390/s19173797

right panel in Figure 4 which shows that except for 10rps , the remaining rates had ITR values around 20-23bpm. 10rps had low TR-VEP performance and low ITR around 14bpm with single sweep data.

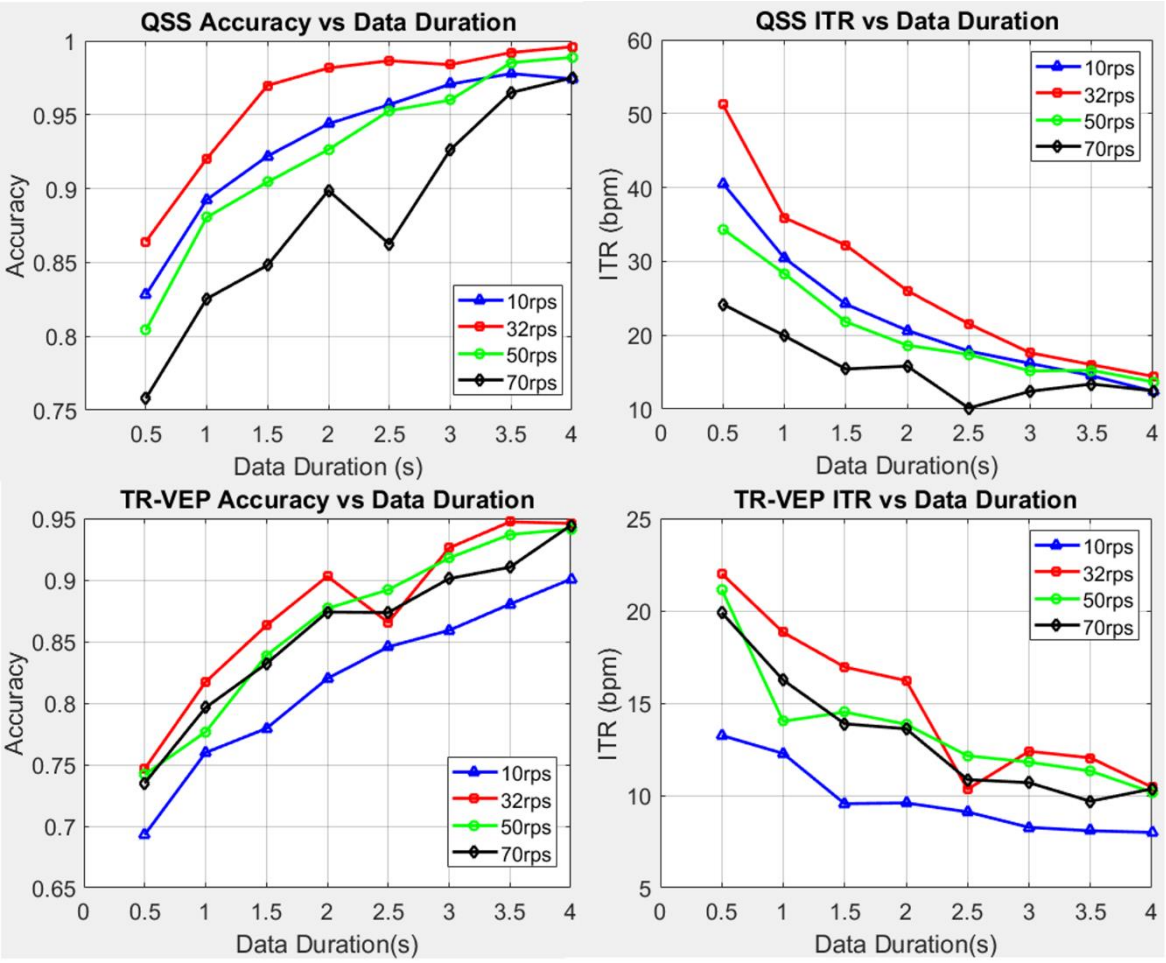

Figure 4. QSS-VEP performances for left and right gazes were averaged as single QSS-VEP performance parameter at each rate. 32rps had the highest accuracy and ITR performance ($p<0.05$) with QSS-VEP signature while 70rps had the lowest performance ($p<0.05$). For the 8 Subject population average ITR values for QSS-VEP (top-right) and TR-VEPs (bottom-right) were plotted for each rate and data durations.

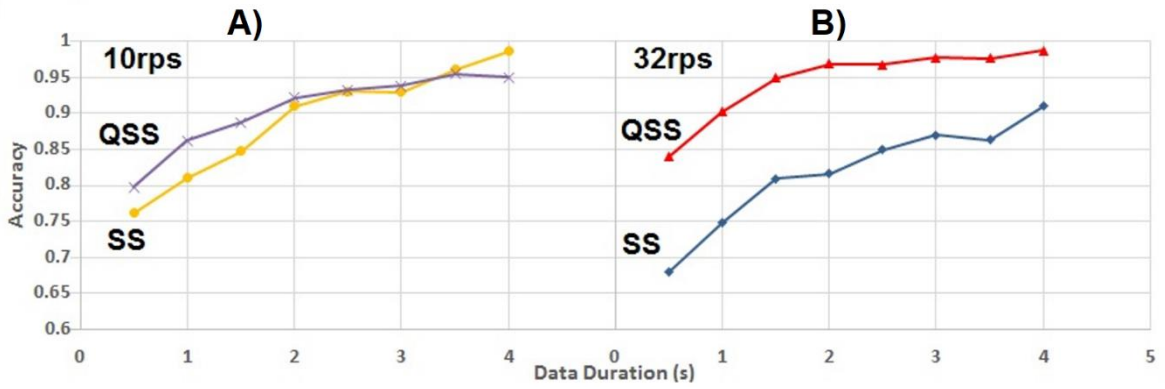

Figure 5. QSS-VEP and SSVEP performances are compared. A) 10rps QSS vs SS VEP accuracies. B) 32rps QSS vs SS VEP accuracy performances are compared.

When QSS and Steady State (SS) performances were compared, QSS-VEP 10rps accuracy was lower than QSS-VEP 32rps accuracy but bigger than both SS 10rps and 32rps accuracies ($p<0.05$) for 0.5s data duration as seen in Figure 5. 32rps SS performed much lower than 10rps SS ($p<0.05$) for 0.5s and 1s data. However after 3s data, they all reached a similar value except for 32rps SS, which was below the rest. On the other hand QSS-VEP 32rps paradigm on the average had 23.5% higher accuracy than the SSVEP paradigm for 0.5s data. Similarly 10rps QSS-VEP paradigm also had 5% higher accuracy performance than the SSVEP paradigm accuracy performance for single sweep data.

4. Discussion

Although SSVEP based BCIs demonstrated their excellence in ITRs, performances of pattern-reversal c-VEP and transient-VEP based BCIs can be improved by researches. Since there is limited number of studies with pattern-reversal VEP, we proposed a research into different reversal rates and the template matching performance of the pattern reversal c-VEP or particularly low jittered QSS-VEPs. For TR-VEP ROC comparisons 10rps performed low compared to other rates. This might be attributed to the interference with alpha band at 10rps. There existed a huge subject variability in the accuracies and ITRs. It was found that user variation could be reduced by selecting the channel location, the stimulus frequency, and the speed of selection parameters carefully [3]. Another source of variation could be attendance and cooperation during the particular tasks, if the user lacked attention during target gazing, the resultant target VEP characteristics would be affected hence accuracy and ITRs would be influenced adversely for these tasks. However on the overall performance 32rps QSS-VEP paradigm led to highest accuracy values and ITRs in offline analysis compared to 10rps, 50rps and 70rps reversal rates. One of the reasons behind this is that the number of visible peaks with 32rps stimulation in the resultant QSS-VEP is higher than the number of visible peaks with other QSS stimulation rates. However at 50rps and 70rps due to convolution and superposition of transient VEPs , the resulting QSS-VEPs did not elicit that many peaks contributing to template matching. Another aspect of the research was comparison of SSVEP to QSS-VEP in template matching accuracy. As mentioned before SSVEPs had smaller peaks at high rates [22]. QSS-VEPs on the other hand had multiple peaks and higher amplitudes compared to SSVEPs.

QSS stimulation improves the SNR performance due to jitter in the paradigm and this jitter cancels out adverse effects of adaptation on signal peaks. QSS-VEP generates larger peaks at higher rates where steady state responses are diminished by adaptation. The low jitter design of QSS stimulation allows the extraction of base TR-VEPs responses. If TR-VEPs have bigger amplitude at particular rates, it is due to the boosting effect of special QSS stimulation. As compared QSS-VEPs at 32rps performed significantly ($p<0.05$) better than 32rps SS counterparts for 1,2 or 3 sweeps averages. Similarly 10rps QSS stimulation performed better than 10rps SS for 1,2 or 3 sweeps.

5. Conclusions

This research revealed that QSS-VEP paradigm offers a feasible alternative to the methods applied to c-VEP or SSVEP based BCIs. The advantages of the QSS-VEP method are that it increases accuracy of the SSVEP template matching at the same reversal rates, it enables extraction of clinically significant TR-VEP from low jittered QSS-VEPs. By special design of low jitter QSS sequences, it was possible to enhance SNR and accuracy at higher rates compared to rates interfering with alpha band. 32rps achieved the maximum boosting effect by the QSS-VEP, which led to higher accuracy performances in template matching based dual target BCI switch.

Supplementary Materials: The following is available online at www.mdpi.com/xxx/s1, Table S1: Single Sweep QSS-VEP Accuracy and SNR values for all subjects.

Author Contributions: Conceptualization, I.K, J.B., O.O; methodology, I.K., J.B., O.O; software, I.K.; validation, I.K.; formal analysis, I.K.; investigation, I.K.; resources, J.B; data curation, I.K.; writing—original draft preparation, I.K.; writing—review and editing, I.K., J.B, O.O.; visualization, I.K.; supervision, J.B., O.O.; project administration, O.O.

Conflicts of Interest: The authors declare no conflict of interest.

References

1. Wang, Y., Gao, X., Hong, B., Jia, C., & Gao, S. Brain-computer interfaces based on visual evoked potentials. *IEEE Eng. Med. Biol. Mag.* **2008**, *27(5),* 64-71. https://doi.org/10.1109/MEMB.2008.923958
2. Nicolas-Alonso, L. F., & Gomez-Gil, J. Brain computer interfaces, a review. *Sensors* **2012**, *12(2),* 1211-1279. https://doi.org/10.3390/s120201211
3. Wang, Y., Wang, R., Gao, X., Hong, B., & Gao, S. A practical VEP-based brain-computer interface. *IEEE Trans. Neural Syst. Rehabil. Eng.* **2006**, *14(2),* 234-240. https://doi.org/10.1109/TNSRE.2006.875576
4. Odom, J.V., Bach, M., Brigell, M., Holder, G. E., McCulloch, D.L., Mizota, A., Tormene, A. P. "ISCEV standard for clinical visual evoked potentials-(2016 update)". *Doc. Ophthalmol.* **2016** *133(1):* 1-9. https://doi.org/10.1007/s10633-016-9553-y
5. Fahle M Bach M . Origin of the visual evoked potentials. In: Heckenlively JR Arden GB eds. *Principles and Practice of Clinical Electrophysiology of Vision*. Cambridge, MA: The MIT Press; **2006**;207–234.
6. Sokol, S. "Visually evoked potentials: theory, techniques and clinical applications." *Surv. Ophthalmol.* **1976**, 21(1), 18-44. https://doi.org/10.1016/0039-6257(76)90046-1
7. Zemon, V. M., & Gordon, J. Quantification and statistical analysis of the transient visual evoked potential to a contrast-reversing pattern: A frequency-domain approach. *Eur. J. Neurosci.* **2018**, *48(2),* 1765-1788. https://doi.org/10.1111/ejn.14049
8. Özdamar, Ö., & Bohórquez, J. Signal-to-noise ratio and frequency analysis of continuous loop averaging deconvolution (CLAD) of overlapping evoked potentials. *JASA* **2006**, *119(1),* 429-438. https://doi.org/10.1121/1.2133682
9. Capilla, A., Pazo-Alvarez, P., Darriba, A., Campo, P., & Gross, J. Steady-state visual evoked potentials can be explained by temporal superposition of transient event-related responses. *PloS one* **2011**, *6(1),* e14543. https://doi.org/10.1371/journal.pone.0014543
10. Regan, D. Steady-state evoked potentials. *J. Opt. Soc. Am.* **1977,** *67(11),* 1475-1489. https://doi.org/10.1364/JOSA.67.001475
11. Bin, G., Gao, X., Wang, Y., Hong, B., Gao, S. "VEP-based brain-computer interfaces: time, frequency, and code modulations [Research Frontier]." *IEEE Comput. Intel. Mag.* **2009**, *4(4)* : 22-26 https://doi.org/10.1109/MCI.2009.934562
12. Chen, X., Chen, Z., Gao, S., & Gao, X. Brain–computer interface based on intermodulation frequency. *J. Neural Eng.* **2013**, *10(6*), 066009. https://doi.org/10.1088/1741-2560/10/6/066009
13. Cheng, M., Gao, X., and Gao, S. Design and implementation of a brain–computer interface with high transfer rates. *IEEE Trans. Biomed. Eng.* **2002**, *49* 1181–6. https://doi.org/10.1109/TBME.2002.803536
14. Gao, X., Xu, D., Cheng, M. and Gao, S. A BCI-based environmental controller for the motion-disabled. *IEEE Trans. Neural Syst. Rehabil. Eng.* **2003**, *11* 137–40. https://doi.org/10.1109/TNSRE.2003.814449
15. Li, Y., Bin, G., Gao, X., Hong, B. and Gao, S. Analysis of phase coding SSVEP based on canonical correlation analysis (CCA). *Proc. 5th Int. IEEE/EMBS Conf. Neural Eng*. **2011,** pp 368–71 https://doi.org/10.1109/NER.2011.5910563
16. Jia, C., Gao, X., Hong, B. and Gao, S. Frequency and phase mixed coding in SSVEP-based brain–computer interface. *IEEE Trans. Biomed. Eng.* **2011**, *58* 200–6. https://doi.org/10.1109/TBME.2010.2068571
17. Bin, G., Gao, X., Wang, Y., Li, Y., Hong, B., Gao, S. "A high-speed BCI based on code modulation VEP." *J. Neural Eng.* **2011**, *8*(2): 025015. https://doi.org/10.1088/1741-2560/8/2/025015
18. E. E. Sutter, "The brain response interface: communication through visually-induced electrical brain responses," *J. Microcomput. Appl.* **1992**, 15 pp.31-45. https://doi.org/10.1016/0745-7138(92)90045-7
19. Bohórquez, J., & Özdamar, Ö. Signal to noise ratio analysis of maximum length sequence deconvolution of overlapping evoked potentials. *JASA* **2006**, 119(5), 2881-2888. https://doi.org/10.1121/1.2191609
20. Toft-Nielsen, J., Bohórquez, J., & Özdamar, Ö. Unwrapping of transient responses from high rate overlapping pattern electroretinograms by deconvolution. *Clinical Neurophysiology* **2014** 125(10), 2079-2089. https://doi.org/10.1016/j.clinph.2014.02.002

21. Bohórquez, J., Lozano, S., Kao, A., Toft-Nielsen, J., & Özdamar, Ö. Deconvolution and modeling of overlapping visual evoked potentials. *In 29th IEEE Southern Biomed. Eng. Conf.* **2013, May**. (pp. 31-32). https://doi.org/10.1109/SBEC.2013.24
22. Diez, P. F., Müller, S. M. T., Mut, V. A., Laciar, E., Avila, E., Bastos-Filho, T. F., & Sarcinelli-Filho, M. Commanding a robotic wheelchair with a high-frequency steady-state visual evoked potential based brain–computer interface. *MED. ENG. PHYS.*, **2013**, *35(8)*, 1155-1164. https://doi.org/10.1016/j.medengphy.2012.12.005
23. Kaya, I., Bohorquez, J. E., & Ozdamar, O. Brain Computer Interface Switch Based on Quasi-Steady-State Visual Evoked Potentials. In 9th Int. IEEE/EMBS Conf. on Neural Eng. (NER) (**2019, March)** (pp. 1175-1178). IEEE. https://doi.org/10.1109/NER.2019.8716894
24. Heinrich, S. P., & Bach, M. Adaptation dynamics in pattern-reversal visual evoked potentials. *Documenta Ophthalmologica*, **2001**, *102(2)*, 141-156. https://doi.org/10.1023/A:1017509717071
25. Thompson, D. E., Stefanie, B. M., Jane, E. H. "Performance assessment in brain-computer interface-based augmentative and alternative communication." *Biomed. Eng. Online* **2013** *12(1)* : 43 https://doi.org/10.1186/1475-925X-12-43
26. Vialatte, F. B., Maurice, M., Dauwels, J., & Cichocki, A. Steady-state visually evoked potentials: focus on essential paradigms and future perspectives. *Prog. Neurobiol.* **2010**, *90(4)*, 418-438. https://doi.org/10.1016/j.pneurobio.2009.11.005

398 **Supplementary**

399 **Table S1.** Single sweep (0.5s) QSS-VEP accuracy, ITR, SNR and RMS values for all rates and subjects.

		Subject ID															
		Single Sweep (0.5s) Accuracy								ITR (bpm)							
Rate	Classification	S1	S2	S3	S4	S5	S6	S7	S8	S1	S2	S3	S4	S5	S6	S7	S8
10rps	QSS-Left Accuracy	0.83	0.91	0.76	0.83	0.76	0.89	0.71	0.63	42.18	65.65	23.61	41.35	25.00	61.10	15.91	5.65
	QSS-Right Accuracy	0.79	0.92	0.69	0.80	0.72	0.95	0.61	0.71	31.25	73.45	12.82	33.61	18.01	83.62	4.07	15.29
32rps	QSS-Left Accuracy	0.85	0.92	0.80	0.82	0.80	0.92	0.71	0.79	46.52	70.48	34.09	37.61	32.65	72.16	16.22	31.71
	QSS-Right Accuracy	0.89	0.93	0.78	0.81	0.85	0.96	0.71	0.85	59.29	75.64	29.66	36.33	45.33	93.16	15.91	46.82
50rps	QSS-Left Accuracy	0.89	0.85	0.73	0.78	0.76	0.82	0.65	0.84	58.58	46.52	19.54	29.44	24.60	37.61	8.02	42.74
	QSS-Right Accuracy	0.78	0.83	0.66	0.84	0.79	0.87	0.71	0.86	28.78	41.08	8.91	43.31	31.25	53.44	15.45	48.95
70rps	QSS-Left Accuracy	0.92	0.88	0.60	0.72	0.68	0.72	0.62	0.83	70.48	55.45	3.49	16.86	10.83	17.84	4.62	40.26
	QSS-Right Accuracy	0.77	0.85	0.66	0.77	0.61	0.86	0.51	0.77	26.64	47.42	8.91	25.81	4.30	48.95	0.03	26.43
	Average	0.84	0.89	0.71	0.80	0.75	0.87	0.65	0.78	45.46	59.46	17.63	33.04	24.00	58.49	10.03	32.23
		SNR (dB)								Average QSS-VEP RMS (µV)							
Rate	Signal	S1	S2	S3	S4	S5	S6	S7	S8	S1	S2	S3	S4	S5	S6	S7	S8
10rps	QSS-VEP Left	20.63	20.75	14.90	12.32	13.72	16.09	13.98	10.77	4.98	3.85	3.25	2.26	2.51	4.67	2.22	1.81
	QSS-VEP Right	18.06	20.28	15.73	19.48	14.92	18.59	14.47	14.39	4.48	3.82	3.61	2.12	2.56	4.90	2.20	1.91
32rps	QSS-VEP Left	14.50	16.65	13.53	16.29	9.79	16.04	6.46	16.14	4.10	4.45	4.07	2.28	2.71	4.80	2.33	2.68
	QSS-VEP Right	14.40	14.75	12.61	14.90	14.91	16.85	7.00	9.90	3.26	4.60	3.44	1.95	3.02	5.15	2.23	3.04
50rps	QSS-VEP Left	15.95	13.56	9.00	15.83	12.72	11.19	7.11	15.17	4.75	2.86	3.34	2.17	2.22	3.19	1.77	3.08
	QSS-VEP Right	19.14	16.34	10.33	14.37	13.78	11.96	5.27	16.98	4.38	2.84	3.05	2.20	2.63	3.17	1.65	3.25
70rps	QSS-VEP Left	14.00	15.52	3.66	8.60	9.48	8.40	6.15	8.94	4.30	3.36	1.95	1.20	2.09	2.37	1.53	2.02
	QSS-VEP Right	11.81	10.17	8.42	9.94	6.88	10.31	2.83	12.42	2.89	3.38	2.85	1.38	1.61	2.77	1.41	2.10
	Average	16.06	16.00	11.02	13.97	12.03	13.68	7.91	13.09	4.32	3.68	3.24	2.03	2.53	4.04	1.99	2.54

400